Acta metall. Vol. 34, No. 8, pp. 1625–1641, 1986
Printed in Great Britain

0001-6160/86 $3.00 + 0.00
Pergamon Journals Ltd

M.L.T.Y

79

KINETICS OF MARTENSITIC TRANSFORMATION INDUCED BY A TENSILE STRESS PULSE

N. N. THADHANI†

Division of Engineering and Applied Science/Materials Science, California Institute of Technology, Pasadena, California, U.S.A.

and

M. A. MEYERS‡

Center for Explosives Technology Research, New Mexico Institute of Mining and Technology, Socorro, New Mexico, U.S.A.

(*Received* 14 *December* 1984; *in revised form* 11 *October* 1985)

Abstract—The kinetics of martensitic transformation induced by a tensile stress pulse (generated by the reflection of a compressive shock wave at a free surface) in time durations in the microsecond range, were studied in an Fe-32wt%Ni-0.035wt%C alloy. The tensile hydrostatic component of stress interacts with the dilatational strain (~0.04) of the martensitic transformation and increases the M_s temperature. Shock waves were produced by normal impact of a projectile on a target in a one-stage gas gun. Impact experiments were conducted by varying either the temperature (−10 to −50°C), or pulse duration (0.22–1.76 μs) at a constant pressure. The martensitic transformation, normally considered to be athermal in Fe–Ni–C alloys, exhibits an isothermal nature in the microsecond regime. The fraction transformed increases with decrease in temperature at a constant pulse duration, and increase in pulse duration at a constant temperature. The mean volume of the lenticular martensite was found to be constant throughout the progress of the transformation, consistent with the autocatalytic spreading of clusters. The activation energies for $\gamma \rightarrow \alpha'$ transformation in the Fe 32wt%Ni 0.035wt%C alloy, calculated with a modified version of Pati and Cohen's kinetic equation [*Acta metall.* **17**, 189 (1969)], range from 38,000 J/mol at −10°C to 25,000 J/mol at −60°C. The activation energies are linearly related to the total driving force (chemical free energy change + mechanical work due to the transformation). The activation volume for the transformation was calculated and found to be equal to approximately 60 atoms (0.7 nm^3). This indicates that the martensitic nucleation in this alloy, and under the imposed stress conditions, is interface-mobility controlled.

Résumé—Nous avons étudié dans un alliage Fe 32%Ni–0,035%C (en poids) la cinétique de la transformation martensitique induite par une impulsion de la contrainte de traction (produite par le réflexion d'une onde de choc de compression à la surface libre) d'une durée de l'ordre de la microseconde. la composante hydrostatique de traction de la contrainte interagit avec la dilatation (~0,04) de la transformation martensitique et augmente la température M_s. Les ondes de choc étaient produites par l'impact normal d'un projectile sur une cible dans un canon à gaz à un étage. Nous avons effectué des expériences d'impact en modifiant soit la température (−10 à −50 C), soit la durée de l'impulsion (0,22 à 1,76 μs) pour une pression donnée. La transformation martensitique, généralement considérée comme athermique dans les alliages Fe–Ni–C, présente une nature isotherme dans le régime de la microseconde. La fraction transformée augmente lorsqu'on abaisse la température pour une durée d'impulsion donnée et lorsqu'on augmente la durée de l'impulsion pour une température donnée. Le volume moyen de la martensite lenticulaire était constant lors du déroulement de la transformation, ce qui est compatible avec un étalement autocatalytique des amas. Les énergies d'activation de la transformation $\gamma \rightarrow \alpha'$ dans l'alliage Fe–32%Ni–0,035%C (en poids), calculées à l'aide d'une version modifiée de l'équation cinétique de Pati et Cohen, [*Acta metall.* **17**, 189 (1969)] allaient de 38.000 J/mol à −10 C à 25.000 J/mol à −60°C. Les énergies d'activation sone reliées linéairement à la force motrice totale (changement d'énergie libre chimique + travail mécanique dû à la transformation). Nous avons calculé le volume d'activation pour la transformation et nous l'avons trouvé approximativement égal à 60 atomes (0,7 nm^3). Ceci montre que la germination martensitique est contrôlée par la mobilité de l'interface dans cet alliage prus les conditions de contrainte imposée.

Zusammenfassung—Die durch einen Zugspannungspuls (erzeugt durch Reflektion einer kompressiven Stoßwelle an einer freien Oberfläche) im Zeitbereich von Mikrosekunden induzierte martensitische Umwandlung wurde wurde hinsichtlich ihrer Kinetik an der Legierung Fe-32 Gew.-%Ni–0,035 Gew.-%C untersucht. Die hydrostatische Zugkomponente der Spannung wechselwirkt mit der Dilatationsverzerrung (~0,04) der martensitischen Umwandlung und erhöht M_s-Temperatur. Die Stoßwellen wurden durch senkrechten Aufprall eines Projektils auf ein Ziel in einem einstufigen Gasgewehr erzeugt. Diese Versuche wurden durchgeführt entweder in Abhängigkeit von der Temperatur (−10 bis −50°C) oder von der

†Work done in partial fulfillment of the degree of Doctor of Philosophy at New Mexico Institute of Mining and Technology.
‡Present address: U.S. Army Research Office, Research Triangle Park, NC 27709, U.S.A.

Pulsdauer (0,22 bis 1,76 μs) bei konstantem Druck. Die üblicherweise in Fe–Ni–C-Legierungen als athermisch angesehene martensitische Umwandlung zeigt eine isotherme Natur im Mikrosekundenbereich. Der umgewandelte Anteil nimmt zu mit sinkender Temperatur, bei konstanter Pulsdauer, und mit zunehmender Pulsdauer, bei konstanter Temperatur. Das mittlere Volumen des linsenförmigen Martensits bleibt während des Ablaufes der Umwandlung konstant. Dieser Befund ist verträglich mit einem autokatalytischen Ausbreiten von Clustern. Die Aktivierungsenergien Umwandlung $\gamma \rightarrow \alpha'$ in der untersuchten Legierung wurde mit einer modifizierten Version der kinetischen Gleichung von Pati und Cohen [*Acta metall.* **17**, 189 (1969)] berechnet: zu 38000 J/Mol bei -10°C bis zu 25100 J/Mol bei -60°C. Die Aktivierungsenergien hängen linear mit der gesamten treibenden Kraft (Änderung der chemischen freien Energie + mechanische, durch die Umwandlung geleistete Arbeit) zusammen. Das Aktivierungsvolumen für die Umwandlung wurde zu ungefähr 60 Atomolumina (0,7 nm^3) berechnet. Dieses Ergebnis weist darauf hin, daß die martensitische Keimbildung in dieser Legierung unter den angelegten Spannungsbedingungen von der Beweglichkeit an der Grenzfläche kontrolliert wird.

1. INTRODUCTION

The martensitic transformation has been generally classified, according to the observed kinetic behavior, into isothermal and athermal [1–3]. While the fraction of martensite formed increases with time, at a constant temperature, for the isothermal case, it is considered constant for athermal martensite, in which it is a function of under-cooling below M_s. There have been proposals [4, 5] that athermal martensite is an ultrafast isothermal transformation. In many martensitic systems, the isothermal component is either obscured by the predominant athermal behavior or is operative on a very small time scale which makes it virtually impossible to detect the beginning and progress of the phenomenon. However, today there are numerous examples of isothermal reactions [1–13], ruling out the athermal mode as the necessary manifestation of martensitic reactions.

The effect of externally applied stresses on the formation of martensite was first observed by Scheil [14]. In 1953, Patel and Cohen [15] systematically investigated this effect and found that shear stresses help the transformation and normal stresses favor or oppose it depending on whether they were tensile or compressive, respectively. Hence, uniaxial tensile and compressive stresses favor the transformation and raise the M_s temperature, while hydrostatic compression stresses oppose the transformation and lower the M_s (martensite start) temperature. They proposed a rationale based on the interaction of externally applied stresses and the strains generated by the martensitic transformation (dilatational strain of 0.04 and shear strain of 0.18); one can infer from their rationalization that hydrostatic tensile stresses should also help the transformation and increase M_s.

Meyers and Guimarães [16] in 1976 found that tensile pulses produced by the reflection of shock waves at a free surface generated martensite in a Fe–Ni–C alloy, while compressive waves only produced dislocations. Snell *et al.* [17] also observed martensitic transformation in disc-shaped Fe–Ni–C alloy, flyer plate samples impacted at room temperature. The transformed phase was formed preferentially near the free surface of the discs. Later, Meyers [18] showed that this distribution of martensite in the experiments by Snell *et al.* [17] was due to the tensile pulse and used this interpretation to estimate the nucleation time for martensite.

In the present work a new technique, utilizing tensile stress pulses with time durations of the order of fractions of microseconds, is introduced. The objective was to generate conditions favourable for martensite formation in the submicrosecond range, in order to gain a better understanding of the kinetics of γ–α' transformation.

2. EXPERIMENTAL

A well characterized alloy used in a previous investigation [19] and known to exhibit athermal burst behavior was used in this study. Its chemical composition was analysed to be Fe–32wt%Ni–0.035wt%C. The alloy, received in the form of a 15.5 mm plate, was rolled down to 10.0 and 5.5 mm by successive passes and annealed at 1100°C for 2 h in a vacuum of the order of 10^{-5} mm Hg. The resulting grain size, as determined by the linear intercept method, was 0.068 mm. The M_s temperature, determined by slowly cooling the alloy and measuring the change in electrical resistivity, was found to be -61°C. The apparatus used for monitoring the temperature and resistivity changes was in essence the one described by Guimarães [20]. The alloy was then machined into disc-shaped specimens and impacted by a flat projectile in a gas gun, at temperatures above M_s.

The impact experiments were conducted at the Poulter Laboratory of SRI-International. A fully instrumented 6.35 cm diameter, one stage gas gun was adapted for the specific needs of the experiments. Figure 1 shows the projectile, driven by high pressure gas, that travels through an evacuated barrel. The head of the projectile consists of a flyer plate backed up by low impedance plastic foam or honeycomb. The target is placed at the end of the barrel, backed up by honeycomb as shown in Fig. 1. The impacted specimen is recovered in an evacuated catcher tank.

The purpose of the impact event was to generate tensile pulses, and not only compressive waves. Hence, the targets were not protected by spall plates, so that the shock wave, on reflection from the back

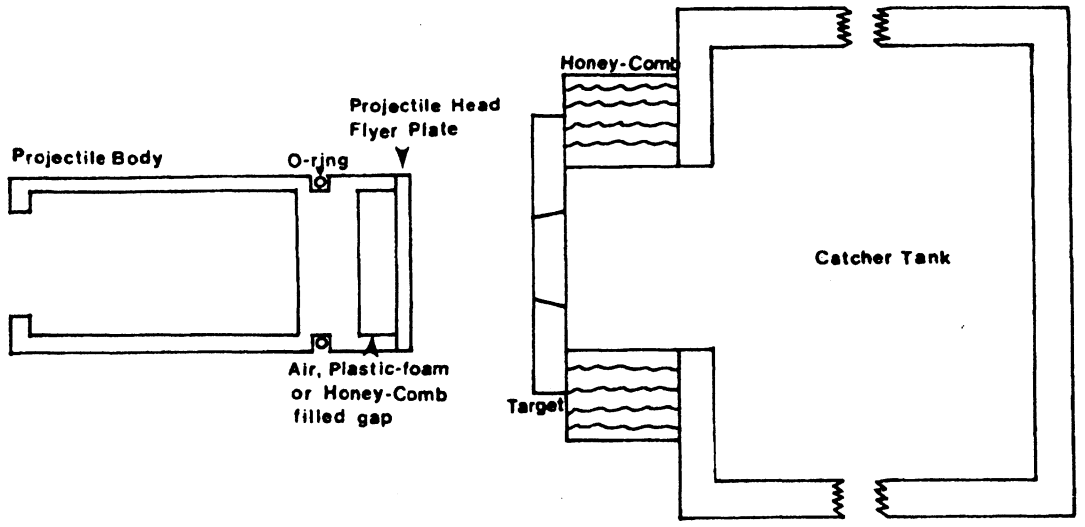

Fig. 1. Schematic representation of the projectile and target used in gas-gun experiments.

(free) surface, would generate a tensile pulse. For most of the experiments performed, AISI 304 stainless steel was used for the flyer plate. However, because of the inconsistent velocities being achieved with stainless steel, the latter experiments were performed with flyer plates of 6061-T6 aluminum alloy. The flyer plate always had a thickness equal to half the target thickness. This ensured that the maximum tensile pulse occurred in the center of the target.

The progress of shock waves throughout a material, produced when a flat flyer plate impacts a target disc, is shown in the stress/distance plots at different time intervals in Fig. 2. At time t_0, the incident shock compression wave (shown as positive) produced at the impact plane, travels inside the flyer and target. The compression wave, on reaching the flyer free surface, reflects back at time t_2 as a release wave. At t_4, the release wave from the flyer crosses the flyer-target interface, and simultaneously the compression wave in the target reflects back as a release wave from the target free surface. These two release waves, on colliding at time t_7, cancel each other and produce a tensile pulse (shown as negative), which propagates through the target. On reaching the flyer-target interface, the tensile pulse reflects back as a recompression wave and, because this interface cannot support tension, the flyer and target separate. The reflected recompression waves once again interact in the center of the target and produce a tensile pulse. This continues until the shock wave attenuates itself during its motion through the target. If the target thickness is twice that of the flyer the tensile pulse is formed in the center of the target. The tensile pulse formed in this manner is responsible for inducing the martensitic transformation.

In order to avoid lateral tensile pulses in the target, the disc-shaped specimen, with a diameter of 30 mm, was inserted (with a 10° taper and pressure fit) in a 90 mm diameter ring. The maximum target thickness with this configuration that assured a uniaxial strain state was 10 mm. When the tension pulse formed in the center of the target (at time t_7 in Fig. 2) approaches the flyer-target interface, there is separation of the central "puck" (target) from the ring. This has to occur before the radial release wave, converging after reflection from the outer surface of the ring, converges inwards and enters the central "puck". If the radial release wave enters the puck before it separates from ring, the uniaxial strain state is disturbed. Hence, the target and projectile geometry were so designed that a uniaxial strain configuration was assured, prior to and during transformation, in the central "puck" (specimen).

Additional causes of concern were (a) the successive tensile pulses in the specimen, after the waves successively reflect at the free surfaces and (b) that the compressive waves might retransform the martensite into austenite. This would have the effect of increasing the duration of the tensile pulse. However, the wave amplitude is attenuated continuously. This is discussed in greater detail by Thadhani [21]. The rate of attentuation is such that no significant additional transformation or transformation reversion should occur.

Cooling of the target to the desired temperature was accomplished by circulating liquid nitrogen through copper coils attached to the back of the external portion of the target. The temperature was continuously monitored by means of an iron–constantan thermocouple welded to the target.

Quantitative metallography was performed to determine the martensite volume fraction transformed and the mean volume per martensite plate. The martensite fraction transformed was determined us-

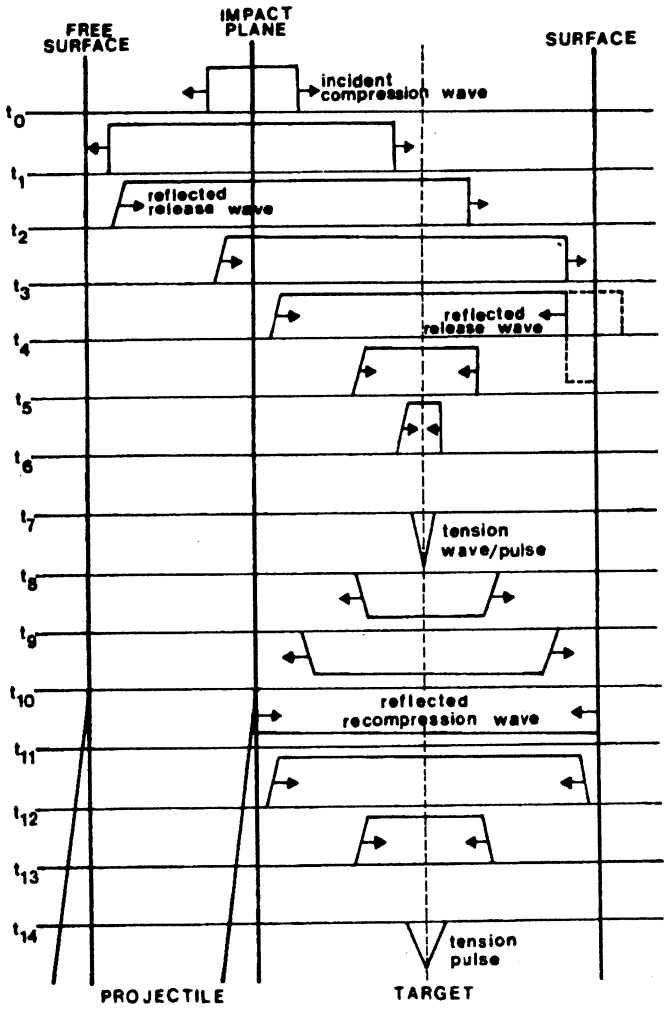

Fig. 2. Schematic showing how a compressive shock wave reflects itself at a free surface, producing a tensile pulse.

ing the point counting technique [22]. In general, ten photo-micrographs at a magnification of 175 × were taken across the central cross-section of each recovered target specimen, and a total of approximately 1000 possible points were counted on each micrograph. The average of fractions computed on each micrograph was considered to be the fraction of martensite transformed (f) in each specimen at the position of maximum pulse duration. The mean volume of a martensite plate ($\bar{v}$) was obtained using Fullman's [23] equation

$$\bar{v} = \frac{\pi^2 f}{8 \bar{E} N_A} \tag{1}$$

where $\bar{E}$ is the mean reciprocal of the plate length as intersected by a random plane, and N_A is the number of martensitic plates per unit area of random cross-section. $\bar{E}$ and N_A were measured on micrographs (blown up to magnification of 700 ×) of specimens impacted under different conditions of pressure, temperature, and duration and containing different amounts of martensite.

3. RESULTS AND DISCUSSION

A summary of the experimental conditions and operating parameters for each gas gun event, and the magnitudes and durations of the tensile pulse at the center of each impacted target are given in Table 1. In order to perform kinetic studies on martensitic transformations induced by tensile stress pulses it is very important to characterize the pulse shape at any distance away from the impact surface in the target discs. The magnitudes and durations of the tensile stress pulses listed in Table 1 for different impact events were computed with the SWAP-7 (Stress Wave Analyzing Program) code, developed by Barker [24]. The detailed description of this code is presented in the Appendix.

Table 1. Experimental conditions and operating parameters for gas-gun events

	Material characteristics			Target specifications		Impact conditions				Results
Shot No.	Flyer material	Specimen thickness (mm) Flyer	Target	M_s temp (°C)	Grain Size (mm)	Impact temp. (°C)	Impact velocity (m/s)	Stress level (GPa)	Pulse duration (μs)	% Martensite transformed
1	Fe–Ni–C	5.0	9.9	−61	0.059	25	162.0	1.6570	3.474	Spall
2	Fe–Ni–C	5.0	9.9	−61	0.059	25	77.0	0.7877	3.474	0.0
3	Fe–Ni–C	5.0	9.9	−61	0.059	25	274.6	2.8065	3.474	Spall
4	304 SS	2.5	5.0	−60	0.068	−30	171.0	1.6570	0.858	Spall
5	304 SS	2.5	5.0	−60	0.068	−30	60.0	0.7879	0.858	36.2 ± 8
6	304 SS	2.5	5.0	−60	0.068	−40	76.5	0.9915	0.857	46.6 ± 9
7	304 SS	2.5	5.0	−60	0.068	−10	86.5	1.1150	0.857	7.0 ± 4
8	304 SS	2.5	5.0	−60	0.068	−50	58.0	0.7633	0.858	47.7 ± 11
9	304 SS	2.5	5.0	−60	0.068	−20	73.7	0.9569	0.858	23.5 ± 11
10	304 SS	2.5	5.0	−54	0.06–0.12	−30	73.2	—	—	[a]
11	304 SS	5.0	9.9	−60	0.068	−30	73.2	0.8592	1.716	40.3 ± 10
12	304 SS	0.625	1.25	−54	0.06–0.12	−30	73.6	—	—	[a]
13	304 SS	1.25	2.5	−54	0.06 0.12	30	85.6	—	—	[a]
14	304 SS	5.0	5.0	−60	0.068	−30	82.6	1.066	0.858	44.7 ± 11
15	304 SS	1.25	2.5	−60	0.068	−30	82.3	1.063	0.429	29.2 ± 8
16	304 SS	0.625	1.25	−60	0.068	−30	91.1	1.172	0.214	27.9 ± 8
17	304 SS	0–8.0	9.9	−60	0.068	−30	95.7	—	—	[b]
18	Fe–Ni–C	2.5	2.5/5.0/5.0	−60	0.068	25	72.8	—	—	[c]
19	Al6061-T6	5.0	9.9	−60	0.068	−40	159.8	1.390	1.762	71.0 ± 5
20	Al6061-T6	3.75	7.5	−60	0.068	−40	157.5	1.366	1.322	66.2 ± 6
21	Al6061-T6	2.5	5.0	−60	0.068	−40	159.7	1.385	0.881	—
22	Al6061-T6	1.25	2.5	−60	0.068	−40	156.0	1.354	0.441	59.8 ± 7
23	Al6061-T6	0.625	1.25	−60	0.068	−40	156.9	1.367	0.221	46.8 ± 7
24	Fe–Ni–C	2.5	2.5/5.0/5.0	−60	0.067	25	90.5	—	—	[c]
25	Al6061-T6	5.0	9.9	−60	0.067	−30	162.2	1.405	1.761	44.6 ± 5
26	Al6061-T6	5.0	9.9	−60	0.067	−20	161.5	1.400	1.762	29.6 ± 5
27	Al6061-T6	5.0	9.9	−60	0.067	−40	161.2	1.397	1.762	73.7 ± 2
28	Al6061-T6	5.0	9.9	−60	0.067	−50	160.6	1.390	1.762	78.1 ± 2
29	Al6061-T6	1.25	2.5	−60	0.067	−20	160.9	1.391	0.441	21.1 ± 4
30	Al6061-T6	1.25	2.5	−60	0.067	−50	159.7	1.385	0.441	64.6 ± 4
31	304 SS	0.625	1.25	−60	0.067	−30	82.9	1.070	0.2143	9.3 ± 3
32	304 SS	5.0	9.9	−60	0.067	−30	79.2	0.9810	1.715	50.3 ± 5
33	Al6061-T6	2.5	5.0	−60	0.067	−40	162.2	1.405	0.880	61.9 ± 3

[a]Incorrect heat treatment.
[b]Slanting flyer plate experiment.
[c]Instrumented gage shot experiment.

3.1. Preliminary exploratory experiments

Patel and Cohen [15] proposed a rationalization for the effect of externally applied stresses (shear + hydrostatic) on M_s. A linear extrapolation of their results showed that a stress level of 0.55 GPa would be sufficient to form martensite at room temperature in the Fe–32wt%Ni–0.035wt%C alloy subjected to uniaxial strain state. The preliminary experiments were performed with a two-fold purpose: (i) to test the correctness of Patel and Cohen's rationalization under dynamic stress conditions, and (ii) to estimate the threshold pressure at which there would be considerable martensite formed, but without spalling. Spalling is a dynamic failure phenomenon [25] and would be undesirable because of the relief waves produced by the generation of new surfaces.

Impact experiments were conducted at ambient temperature on specimens (0.9 mm thick targets) at three different stress levels: 0.8, 1.7 and 2.8 GPa. It was observed that no transformation occurred in the target specimen impacted at 0.8 GPa, whereas calculations based on Patel and Cohen's rationale had predicted that an impact pressure of 0.55 GPa would form martensite. This disagreement can be ascribed to either one or all of the following factors: (a) the constants used in the calculations based on Patel and Cohen's rationalization were determined from the plot, Fig. 3 in Ref. [15], assuming that the extrapolated response would be linear; (b) Patel and Cohen applied a quasistatic hydrostatic state of stress for their computation whereas in this investigation ultrahigh loading rates do not allow sufficient time for transformation; (c) recent results and an analysis of nucleation statistics by Tsuzaki and Olson [26] show that the stress dependence of M_s could be three times higher than Patel and Cohen's prediction, requiring a stress of 1.65 GPa at ambient temperature.

Targets impacted at 1.7 and 2.8 GPa did result in martensite formation. Considerable spalling was also observed in these specimens. The flyer plate (made from same Fe–Ni–C alloy) was always subjected to compressive stresses and showed no transformation to martensite. The effect of impact pressure on the subsequent change in M_s temperature at ambient pressure was studied in the flyer plate. This was done by cooling the flyer plate material and observing the temperature at which martensite stated to form. As shown in Fig. 3, the M_s temperature was observed to change from -61°C, at ambient pressure, to -39°C after impact at a pressure of 2.8 GPa.

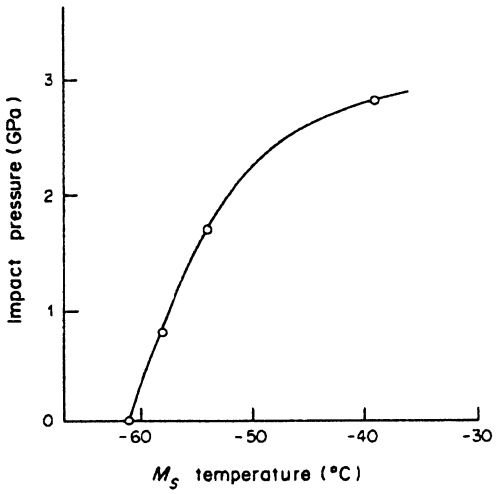

Fig. 3. Variation of the M_s temperature after shock loading with impact pressure.

The results obtained in these preliminary experiments revealed that the predicted value for the stress level required for martensite formation (0.55 GPa at room temperature) was incorrect. Since there was considerable spalling already being observed at pressures greater than 1.7 GPa, it was decided to conduct the subsequent experiments at less than 1.5 GPa and provide additional driving force by stressing at lower temperatures.

3.2. Experiments at varying temperatures

Gas gun impact experiments were conducted as a function of temperature (-10 to -50°C), for pulse durations of 0.44, 0.86 and 1.76 μs, at the constant initial pressure of 1.4 GPa. Figure 4 shows the micrographs of the cross-sections of target specimens impacted at temperatures -10, -20, -30, -40, and -50°C and a maximum pulse duration of 0.86 μs. In these micrographs the martensite regions can be perfectly distinguished from the parent phase because they appear dark.

Very little transformation to martensite is observed in the target specimen impacted at -10°C. However, with further decrease in the temperature of impact, the amount of transformation to martensite is observed to increase. In general, the transformed region appears to be centrally localized in the disc-shaped target specimens. This nonuniform martensite distribution (maximum fraction at center and decreasing towards respective surfaces) agrees precisely with the contention of martensite generated by tensile waves, and with the thickness ratio between the flyer plate and target (1:2). Accordingly, the duration of the tensile pulse is maximum at the center of the target. This implies that tensile pulses (and not compression shock waves) induce the transformation; if it were induced by the compression waves, the region adjoining the impact surface should show the maximum transformation.

Quantitative metallography to determine the volume fraction of martensite transformed was performed on all target specimens. The volume fraction was computed at the position of maximum tensile pulse duration and plotted as a function of temperature. Figure 5 shows the plot of martensite fraction transformed as a function of temperature at pulse durations of 0.44, 0.86 and 1.76 μs. The increase in the amount of martensite transformed with the decrease in temperature is higher as the tensile

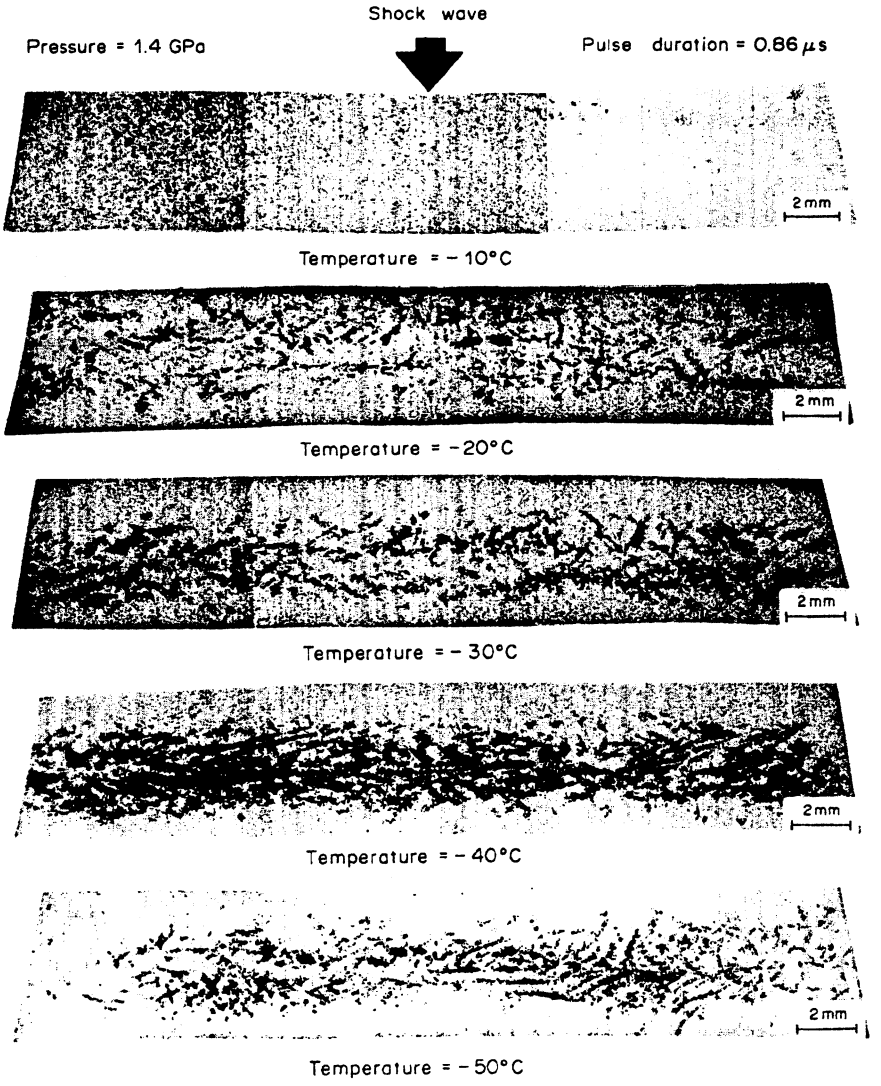

Fig. 4. Micrographs of cross-sections of recovered targets impacted at varying temperatures and constant pulse duration of 0.86 μs.

pulse duration is increased from 0.44 to 1.76 μs. The temperature at which martensite starts forming under the influence of a tensile pulse (of fixed magnitude) can be obtained by extrapolating the curves to intersect the temperature axis in Fig. 5, and is observed to be around −8°C. The reaction becomes easily detectable at temperatures near −10°C. With further lowering in temperature the fraction of martensite formed increases and at −50°C, it corresponds to 0.653, 0.693 and 0.786 for pulse durations of 0.44, 0.86, and 1.76 μs, respectively. This lends strong support to the time dependence of martensitic transformation in Fe–32wt%Ni–0.035wt%C alloy, over the temperature range studied.

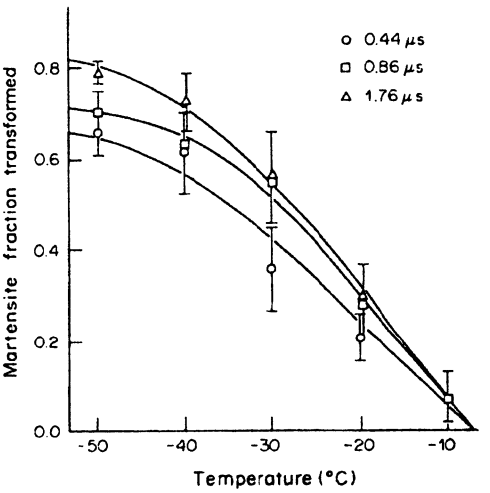

Fig. 5. Variation of martensite fraction transformed with temperature at pulse durations of 0.44, 0.86 and 1.76 μs.

3.3. Experiments at varying pulse durations

An important objective of this investigation was to study the kinetics of martensitic transformation in the

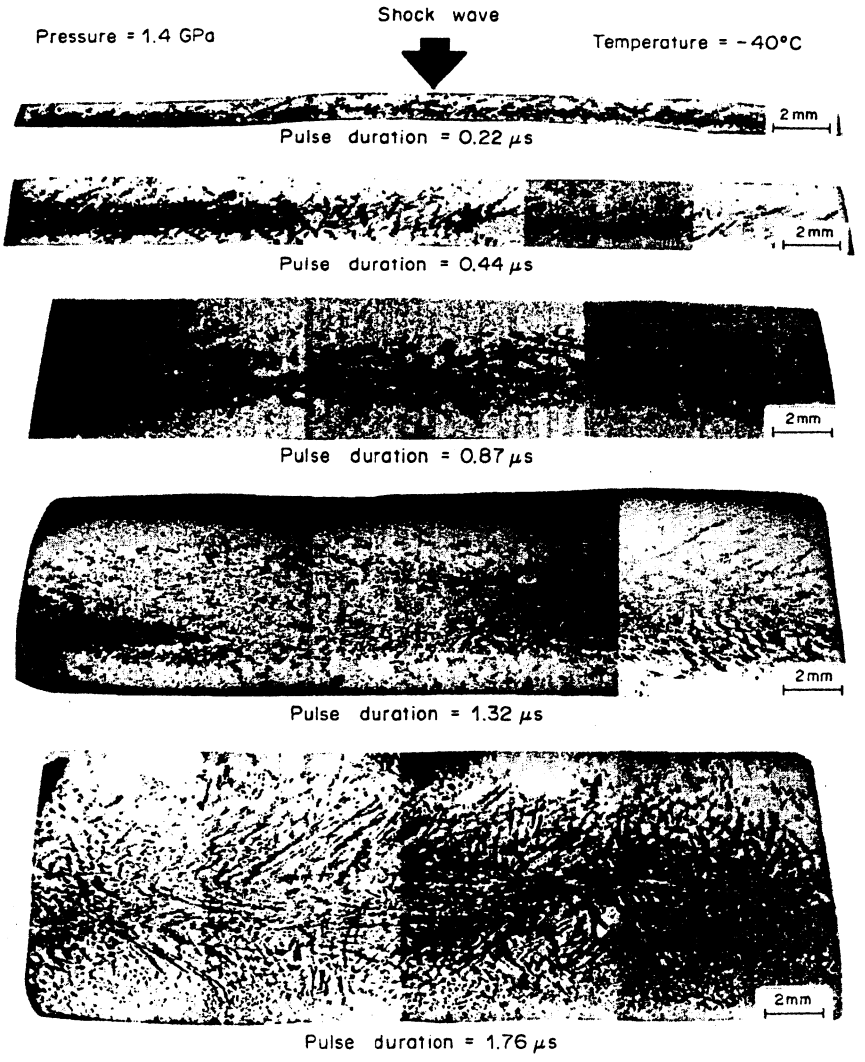

Fig. 6. Micrographs of cross-sections of recovered targets impacted at varying pulse durations and constant temperature of −40°C.

Fe–32wt%Ni–0.035wt%C alloy. For this purpose it was necessary to determine how the fraction transformed changes with time at a constant temperature and stress level. The time can be determined by the duration of the tensile pulse produced on impact, which is a function of the ratio of the flyer plate and target thicknesses.

Figure 6 shows the micrographs of cross-sections of specimens impacted at varying pulse durations, at a temperature of −40°C and constant stress level (1.4 GPa). The thickness of the transformed region, which is localized in the center of the target specimen, is observed to increase as the duration of the tensile pulse increases. The fraction of martensite formed at the position of the maximum duration (center of target), increases with increasing pulse duration. Figure 7 shows the quantitative metallography results for the experiments performed keeping the stress level constant and varying pulse duration (between 0.22

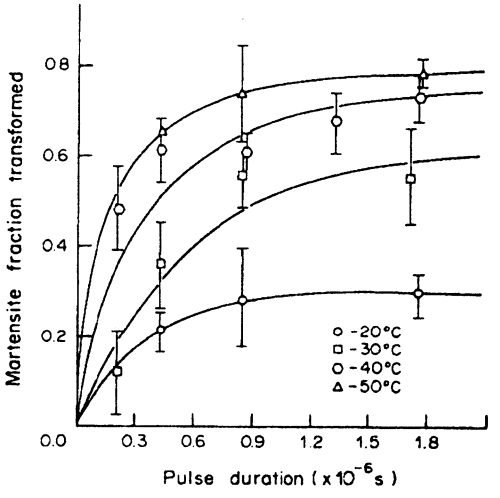

Fig. 7. Variation of martensite fraction transformed with pulse duration at −20, −30, −40, and −50°C.

and 1.76 μs) for the following temperatures: −20, −30, −40 and −50°C. As the temperature is lowered the alloy transforms at a continuously increasing rate to higher and higher final percentages. As is characteristic of Fe–Ni and Fe–Ni–C alloys, the transformation reaches a saturation level. The maximum fraction (or saturation level) of martensite transformed at any temperature increases with the decrease in temperature.

From these results, it can be seen that, over the temperature range studied, isothermal kinetic behavior for the transformation is unquestionably observed. However, this isothermal behavior prevails during time durations of only a few microseconds. At longer durations the transformation characteristics are no longer time dependent. In the micrographs in Figs 3 and 6, the martensite phase appears to form as stringers aligned preferentially along bands. These bands were only observed in impacted specimens and are more pronounced in targets subjected to lower impact pressures. The bands appear to be a consequence of either the shock waves or reflected tensile pulses and are not due to any kind of chemical inhomogeneity or compositional fluctuations. Figure 8 shows the variation in nickel content, obtained by electron microprobe analysis, in the unshocked and shocked specimens. These variations do not account for the regular pattern of bands observed in the material upon impact. One can associate the formation of these bands to inhomogeneous yielding because of work softening undergone during the tensile phase of dynamic loading. The details of this phenomenon are discussed elsewhere [27].

3.4. *Morphology of martensite*

The morphology and distribution of the stress-assisted martensite formed by a tensile stress wave are shown in Fig. 9. The lenticular martensite formed is typical of a bursting alloy having a $[259]_A$ habit plane.

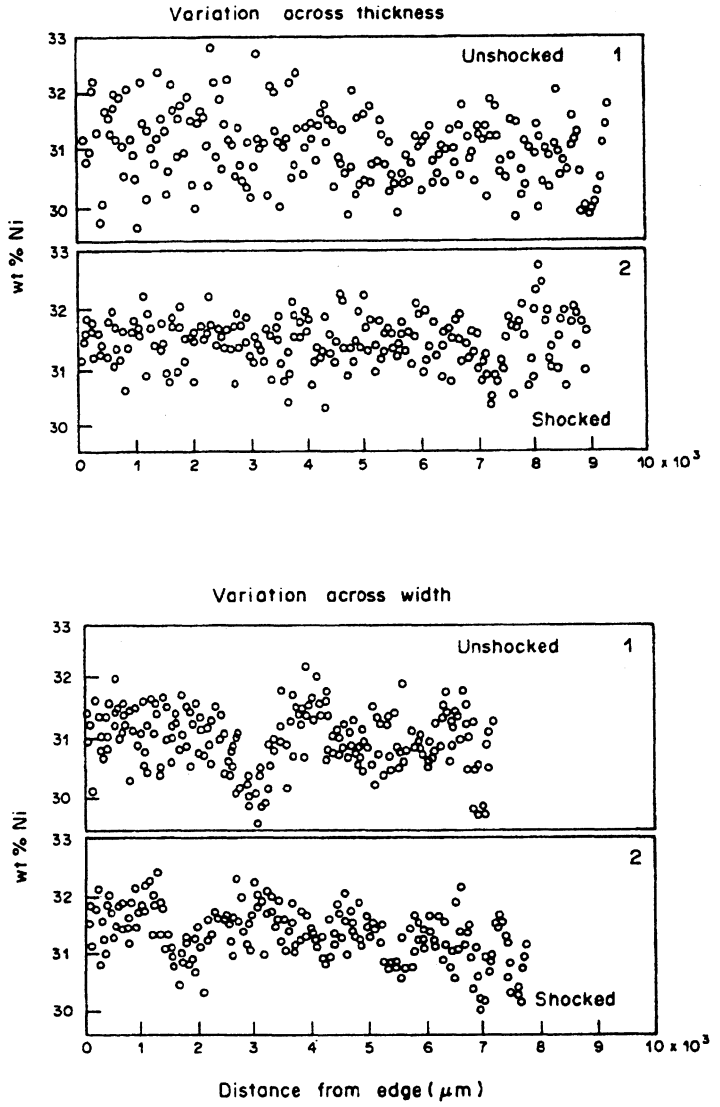

Fig. 8. Variation in the nickel content in an unshocked and shocked specimen.

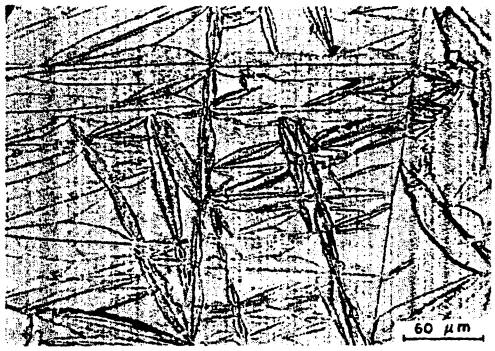

(a)

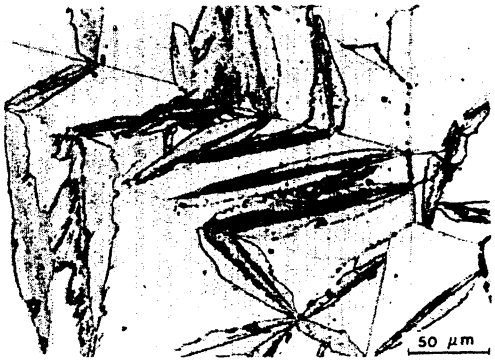

(b)

Fig. 9. (a) Fully grown lenticular martensite with distinct mid-rib and regular interface formed in specimen impacted at −40°C. (b) Stress assisted martensite formed in specimen shocked at 25°C having irregular interface.

The co-operative zig-zag nucleation and growth of these martensitic plates is evident, not only when cooled to temperatures below the M_s temperature, but also on being dynamically stressed below the M_d temperature (Fig. 9). The martensite lenses (or plates) have a highly twinned mid-rib and the width of the twinned layer increases with the decrease in temperature. This is consistent with the observations of Tamura *et al.* [28].

The stress-assisted martensite shown in the micrograph in Fig. 9(a) consists of more regular and fully formed plates than the martensite plates formed at higher temperatures [Fig. 9(b)]. In general, the higher the temperature above the M_s, the more irregular the martensite plate shapes. At higher temperatures the interface gets pinned at the barriers (precipitates) and the driving force is not sufficient to overcome them, resulting in a more irregular shape.

Figure 10 shows the effect of martensite fraction transformed on the mean volume per martensite plate. The variation of mean volume with fraction transformed does not seem systematic, up to about 75% transformation. There have been several proposals in favor of and against this observation [13, 29, 30]. If the "spreading-out" mechanism operates during the early stages of the transformation process, the mean volume per martensite plate can be assumed to be fairly constant. On the other hand if "filling in" prevails, the mean volume decreases as the fraction transformed increases. The results of Fig. 10 indicate that the former mechanism is operating in the Fe–32wt%Ni–0.035wt%C alloy, since no systematic variation in volume is observed.

4. PHYSICAL INTERPRETATION OF TRANSFORMATION KINETICS

4.1. Determination of activation energy

The best equation for describing the kinetics of isothermal martensitic transformations amenable to quantitative metallography is the one given by Pati and Cohen [31]. According to them the transformation rate can be expressed as

$$\dot{f} = \frac{\mathrm{d}f}{\mathrm{d}t} = \left[n_i + f\left(p - \frac{1}{\bar{v}}\right)\right](1-f) \times \nu \exp(-Q_a/RT)\left(\bar{v} + N_v \frac{\mathrm{d}\bar{v}}{N_v}\right). \quad (2)$$

Here, n_i is the total number of available pre-existing nucleation sites, f is the fraction of martensite transformed, p is the autocatalytic factor, $\bar{v}$ is the mean volume per martensite plate calculated from equation (1), ν is the nucleation attempt frequency, and Q_a is the activation energy for nucleation.

Equation (2) is based on the assumption of a single activation energy for all nucleation sites and random nucleation events. It can be modified to accommodate the specific needs of this investigation. If one considers that the mean volume of a martensite plate,

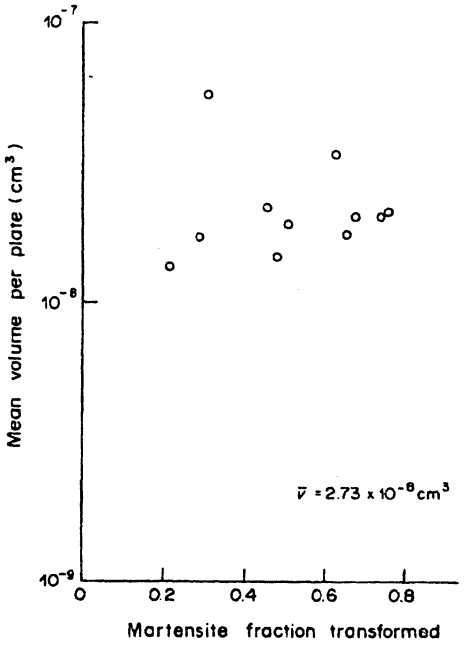

Fig. 10. Variation of the mean volume per martensite plate with fraction transformed.

$\bar{v}$, is not a function of the amount of transformation, then $d\bar{v}/dN_t$ equals zero. This can also be assessed from Fig. 10, which reveals that $\bar{v}$ can be assumed to be approximately constant for the conditions imposed by the tensile stress pulse technique. Eventually the plate size might obviously decrease (during the final stages of the transformation) when clustering is complete and new plates are forced to nucleate within the small pockets of retained austenite. However, the fraction transformed did not exceed 0.8, in the present investigation. Furthermore, the transformation rate expressed by equation (2) is very sensitive to the term $(p - 1/\bar{v})$ on the right hand side of the equation. If $(p - 1/\bar{v}) < 0$, the transformation rate decreases with increasing fraction transformed. Then the reaction ceases after a finite saturation level of transformation is reached at any given temperature. This is the situation observed in the present work for the Fe–32wt%Ni–0.035wt%C alloy, as shown in Fig. 7. The fact that the transformation reaches saturation at a transformed fraction less than one implies that more sites are consumed than are generated by the new plates through autocatalysis; therefore p is small relative to $1/\bar{v}$. Furthermore, the mean volume per martensitic plate is constant and is less than the volume of influence of a nucleation site upon being activated to martensite. These assumptions imply that fewer sites are produced by autocatalysis and that the probability of their falling within the volume of a martensite plate is small. Hence, for p and $\bar{v}$ small and constant, and $(p - 1/\bar{v}) < 0$, the "sweeping-out" effect represented by the term $(1 - f)$ can be reasonably discarded from equation (2) which becomes [32].

$$\dot{f} = \frac{df}{dt} = \left\{\left[n_i + f\left(p - \frac{1}{\bar{v}}\right)\right] \times \nu \exp(-Q_a/RT)\right\}. \quad (3)$$

The initial nucleation rate, assuming that the transformation then occurs from only the pre-existing nucleation sites (i.e. $f = 0$ at $t = 0$), can be expressed as

$$\dot{f}_0 = n_i \bar{v} \nu \exp(-Q_a/RT). \quad (4)$$

As the transformation is allowed to reach completion, the transformation rate, $\dot{f}$, approaches zero; since all the nucleation sites have been consumed, the fraction transformed reaches a saturation value $(f = f_{max})$. Thus, from equation (3)

$$n_i + f_{max}\left(p - \frac{1}{\bar{v}}\right) = 0$$

or

$$\left(p - \frac{1}{\bar{v}}\right) = -n_i/f_{max}. \quad (5)$$

Substituting into equation (3) for $\bar{v}\nu \exp(-Q_a/RT)$ and $p - 1/\bar{v}$ from equations (4) and (5) respectively, one gets

$$\dot{f} = \frac{df}{dt} = \dot{f}_0(1 - f/f_{max}). \quad (6)$$

Rearranging and integrating equation (6) leads to

$$\ln(1 - f/f_{max}) = -(\dot{f}_0/f_{max}) \cdot t. \quad (7)$$

Equation (7) can also be expressed as

$$f = f_{max}\{1 - \exp[(-\dot{f}_0/f_{max}) \cdot t]\}. \quad (8)$$

Equations (7) and (8) express the kinetics of the martensitic transformation under the specific constraints imposed by the experimental conditions of this investigation. Plotting the left hand side term in equation (7) against time, t, as shown in Fig. 11, one gets a slope which is equal to $-\dot{f}_0/f_{max}$. From equation (4), the initial nucleation rate is given as $\dot{f}_0 = n_i \bar{v} \nu \exp(-Q_a/RT)$. Hence, the value of the activation energy, Q_a, can be computed if n_i, $\bar{v}$, ν, and f_{max} are known.

A direct determination of n_i, the initial number of nucleation sites, has not been successfully done, to the present moment. The most widely used estimate of n_i is $10^7\,cm^{-3}$. The mean volume of a martensite plate estimated according to equation (1) was found to be $2.727 \times 10^{-8}\,cm^3$. The nucleation jump frequency, ν, was taken to be $10^{13}\,s^{-1}$, consistent with the model by Pati and Cohen [31]. This is the frequency of atomic vibrations; it is assumed that at each vibration an atom attempts to transform to martensite. The value of $10^{13}\,s^{-1}$ was chosen to maintain consistency with previous kinetic calculations, although recent studies on magnetic field experiments [32] indicate that the vibrational attempt frequency of an interface can be as low as $10^7\,s^{-1}$.

The maximum fraction of martensite that can be formed at any temperature was experimentally determined on a specimen shocked at room temperature

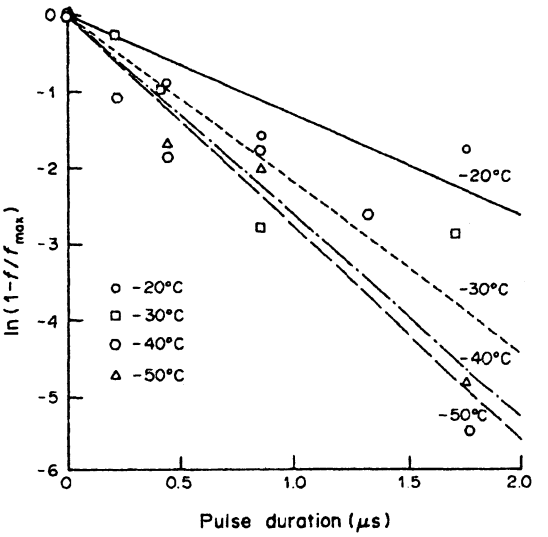

Fig. 11. Plot of $\ln(1 - f/f_{max})$ vs t from impact experiments performed on Fe-32%Ni-0.035%C alloy.

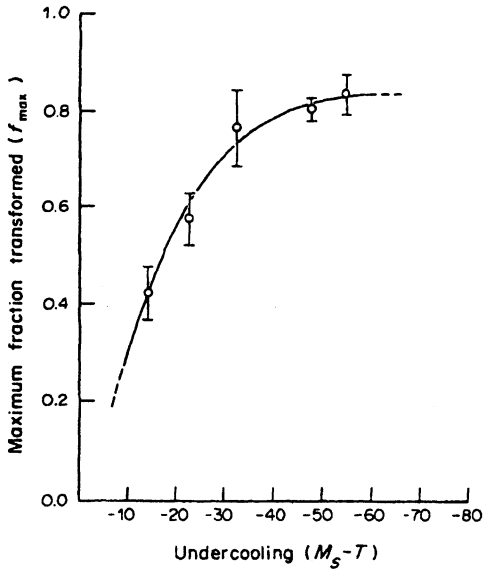

Fig. 12. Maximum martensite fraction (f_{max}) as a function of undercooling (M_s–T) at ambient pressure.

(which did not have any significant transformation produced in the as-shocked state). Several pieces were cut from a flyer plate specimen (subjected to compression stresses only) and each piece was held at different temperatures below M_s (= −55°C after impact at 1.4 GPa pressure), for a sufficiently long time. The maximum fraction of martensite that can be formed as a function of decrease in temperature below this M_s was determined. Figure 12 shows the plot of maximum fraction, f_{max}, as a function of undercooling below the M_s temperature, i.e. M_s–T, at ambient pressure. From the experiments performed at varying temperatures, and constant pulse durations and stress levels, the extrapolated M_s temperature was estimated to be −8°C, as shown in Fig. 5. So, for the difference between this M_s temperature (i.e. the temperature at which martensite starts forming with the application of a tensile pulse), and the temperature of interest, the value of f_{max} can be predicted using the f_{max} vs M_s–T plot in Fig. 12.

Finally, using these calculated and experimentally determined parameters, n_i, $\bar{v}$, ν, f_{max}, and the slope of $\ln(1-f/f_{max})$ vs t in equation (7) (Fig. 11), the activation energy Q_a can be estimated for the different temperatures of interest. The activation energies for the transformation in the Fe–32%Ni–0.035%C alloy determined experimentally lie in the range of 26,000–33,500 J/mol (6200–8000 cal/mol), and are observed to decrease with decrease in temperature as shown in Fig. 13. On extrapolating the Q_a vs T curve in Fig. 13, one can estimate the activation energies at −10 and −60°C. The values for the activation energies are less than half of those previously published by Raghavan and Entwisle [1] and Pati and Cohen [31] for isothermal martensitic transformations, within the temperature range studied in this investigation. These lower activation energies are in fact responsible for the very rapid transformation rates in the Fe–32wt%Ni–0.035wt%C alloy.

One can now go back and substitute the values of Q_a in equation (8) and predict the f vs t transformation curves. Figure 14 shows the agreement between the experimental points and predicted transformation curves for time durations ranging up to 3 μs, and temperatures between −10 to −60°C. Discrepancies can be attributed to the approximation of the transformation being considered to be a singly activated process.

4.2. *Total driving force for $\gamma \rightarrow \alpha'$ transformation*

4.2.1. Chemical free energy change. The chemical free energy change accompanying the transformation in a ternary Fe–Ni–C alloy system based on a subregular solution model can be expressed as [33]

$$\Delta G^{\gamma\rightarrow\alpha'}_{chem} = X_{Fe}\,\Delta G^{\gamma\rightarrow\alpha'}_{Fe} + X_{Ni}\,\Delta G^{\gamma\rightarrow\alpha'}_{Ni} + X_C\,\Delta G^{\gamma\rightarrow\alpha'}_{C} + X_{Ni}X_{Fe}\,\Delta G^{M}_{FeNi} + X_C X_{Fe}\,\Delta G^{M}_{FeC} + X_{Ni}X_C\,\Delta G^{M}_{NiC} \quad (9)$$

where X_{Fe}, X_{Ni}, and X_C are atomic fractions of Fe, Ni, and C respectively; $\Delta G^{\gamma\rightarrow\alpha'}_{Fe}$, $\Delta G^{\gamma\rightarrow\alpha'}_{Ni}$, and $\Delta G^{\gamma\rightarrow\alpha'}_{C}$ are the

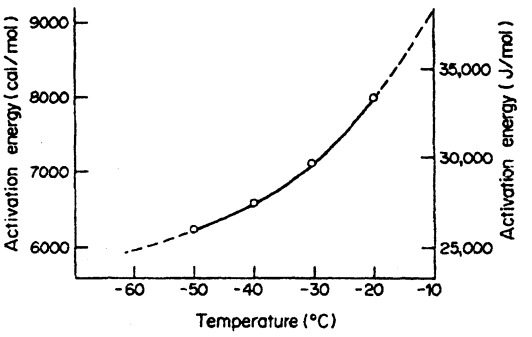

Fig. 13. Variation of activation energy as a function of temperature for Fe–32%Ni–0.035%C alloy.

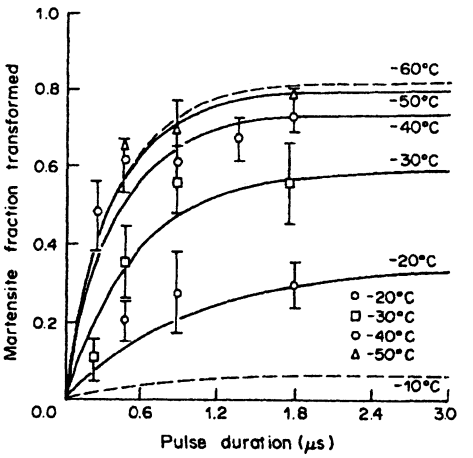

Fig. 14. Agreement between the experimental points and predicted transformation curves for Fe–32%Ni–0.035%C alloy, for temperatures ranging between −10 and −60°C.

free energy differences between the γ and α' phases in Fe, Ni and C respectively; ΔG^{M}_{FeNi}, ΔG^{M}_{FeC} and ΔG^{M}_{NiC} are the excess free energies of mixing. These various terms were estimated using the latest empirical equations of Kaifman and Nesor [34–36].

The values of the chemical driving force accompanying the $\gamma \rightarrow \alpha'$ transformation range from 960 J/mol at -10°C to 1170 J/mol at -60°C.

4.2.2. Mechanical work induced by gas-gun impact. Shear stresses are known to have a strong interaction with the transformation shape strain. Considering some degree of plastic relaxation during the tensile pulse, the thermodynamic effect of stress can become increasingly important. In the Fe–32%Ni–0.035%C alloy the state of stress prevailing during the duration of the tensile pulse can be assumed to be purely elastic. The observed lenticular martensite morphology (Fig. 9) is also evidence of the elastic-stress-assisted martensitic transformation.

The mechanical work contribution to the total driving force for martensite formation can be estimated from the shift in M_s temperature with stress. From Fig. 5 it can be seen that the M_s temperature at 1.4 GPa pressure pulse is -8°C in contrast to the ambient pressure M_s of -61°C.

Using Patel and Cohen's [15] rationalization the mechanical work contribution is expressed as

$$W = \frac{d\Delta G^{\gamma\rightarrow\alpha'}_{chem}}{dT}(\Delta M_s) \qquad (10)$$

where $d\Delta G^{\gamma\rightarrow\alpha'}_{chem}/dT$ is the variation of chemical free energy of transformation with temperature and ΔM_s is the shift in M_s temperature due to the tensile stress pulse. For Fe–32%Ni–0.035%C alloy the mechanical work done with the pressure pulse of 1.4 GPa is 229 J/mol.

4.3. Activation energy dependence on total driving force

Table 2 lists the values of the total driving forces (chemical free energy change and mechanical work) and activation energies for $\gamma \rightarrow \alpha'$ transformation in Fe–32%Ni–0.035%C alloy, determined experimentally for the temperature range -20 to -50°C and extrapolated to -10 and -60°C. Figure 15 shows a plot of driving force versus activation energy. The curve for the Fe–32%Ni–0.035%C alloy lies to the bottom right of the plot and can be expressed as

$$Q_a = 1.82 \times 10^{-12} + 7.18 \times 10^{-22}(\Delta G^{\gamma\rightarrow\alpha'}_{tot}) \text{ J/event.} \qquad (11)$$

Kaufman and Cohen [33] developed a model for the isothermal nucleation of martensite based on the existence of oblate-spheroidal embryos, having a semi-coherent interface, in the parent austenite. This model is based on the Knapp–Dehlinger [38] approach. According to this model the relationship between activation energy, Q_a, and total driving force $\Delta G^{\gamma\rightarrow\alpha'}_{tot}$ can be represented by

$$Q_a = \frac{2.5\pi b^2}{d^2}(\sigma/A)^{1/2}[3\sigma r^{3/2} + \Delta G^{\gamma\rightarrow\alpha'}_{tot}(\sigma/A)^{1/2}r^2] \qquad (12)$$

where b is the Burgers vector, d is the spacing between Frank partials ($2.5\pi b^2/d^2 = 4 \times 10^{-2}$), σ is the interfacial energy, A is the strain energy factor (2.1 kJ/cm^3 [38], and r is the radius of the largest embryo which provides a measure of the "strength" (or the "potency") of a nucleation site. According to equation (12), the activation energy for martensite nucle-

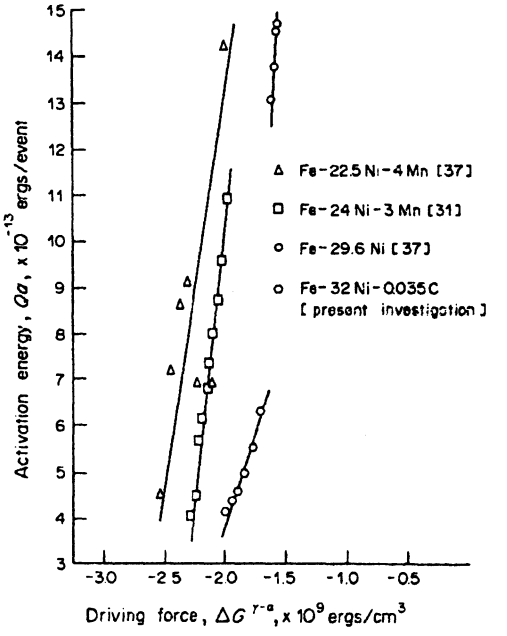

Fig. 15. Activation energy dependence on the total driving force for Fe–32wt%Ni–0.035wt%C alloy.

Table 2. Total driving forces and activation energies for transformation

Temperature (°C)	Chemical driving force (J/mol)	Mechanical work (J/mol)	Total driving force[a] (J/mol)	erg/cm^3 ($\times 10^9$)	Activation energy[b] (J/mol)	erg/event ($\times 10^{-13}$)
−10	960	229	−1189	−1.69	38,074	6.33
−20	1005	229	−1234	−1.76	33,434	5.56
−30	1049	229	−1279	−1.82	29,777	4.95
−40	1092	229	−1321	−1.88	27,488	4.57
−50	1135	229	−1364	−1.94	26,083	4.34
−60	1175	229	−1404	−1.99	24,936	4.15

[a] 1 J/mol = $1.4245 \times 10^{+6}$ ergs/cm^3.
[b] 1 J/mol = 1.6635×10^{-17} ergs/event.

ation should vary linearly with the driving force if the other factors are constant. Comparing equations (11) and (12), one obtains $\sigma = 1500 \times 10^{-7}$ J/cm^2 and $r \simeq 5.0$ *nm*. Here, r is not defined as the actual size of the embryo; rather, it is a measure of the embryo potency.

The relatively small size (potency) of the effective embryo in the Fe–32%Ni–0.035%C alloy as compared to Fe–Ni (42 nm) alloys, [13] is the consequence of lower activation energies required for the transformation. For the same reason the alloy undergoes an ultra-rapid isothermal (time dependent) transformation, and one cannot make an experimental separation between athermal and very rapid isothermal nucleation. Although the Kaufman and Cohen embryo model is outdated, it still provides a good feel for the dependence of the embryo size (potency) on the kinetic behavior (athermal or isothermal) of martensitic transformations.

In Fig. 15, the curves for Fe–29.6%Ni and Fe–22.5%Ni–4%Mn [37], and Fe–24%Ni–3%Mn [31] alloys are also plotted; the original data were changed to be consistent with more recent thermodynamic analyses and attempt frequency (10^{13} s^{-1}) used in the present investigation. The respective Q_a vs $\Delta G_{\text{tot}}^{\gamma\to\alpha'}$ functional relationships for the above three alloys are

$$Q_a = 8.17 \times 10^{-12} + 4.29 \times 10^{-21}(\Delta G_{\text{tot}}^{\gamma\to\alpha'}) \quad (13)$$

$$Q_a = 3.42 \times 10^{-12} + 1.14 \times 10^{-21}(\Delta G_{\text{tot}}^{\gamma\to\alpha'}) \quad (14)$$

$$Q_a = 5.40 \times 10^{-12} + 2.21 \times 10^{-21}(\Delta G_{\text{tot}}^{\gamma\to\alpha'}). \quad (15)$$

The slope ($dQ_a/d\Delta G_{\text{tot}}^{\gamma\to\alpha'}$) of the curves in Fig. 15 is the activation volume for martensitic transformation [39]. Considering an atomic volume of 11.7 Å^3 for a b.c.c. martensite cell, the activation volumes for the different alloys can be converted from cm^3/event to atoms/event. The results are shown in Table 3. Fe–Ni alloys generally have a larger activation volume compared to Fe–Ni–Mn alloys; although the Fe–Ni–C alloy shows a very small activation volume because of the lower activation energy.

It is also interesting to note that in Fig. 15, the curves for Fe–Ni and Fe–Ni–C alloys are located to the right of the Fe–Ni–Mn alloys (i.e. towards lower driving forces). Also, as the Mn content in the Fe–Ni–Mn alloys increases, the curves move further to the left. This is expected since Mn is a strong solid solution strengthener; hence, with increasing Mn one needs a higher driving force to achieve the desired activation energy. For the Fe–Ni and Fe–Ni–C alloys, it appears that a single master curve can be drawn to pass through the two curves shown in Fig. 15. The generalized curve would in fact possess some curvature, especially as lower activation energies are approached. The experiments performed on Fe–32%Ni–0.035%C alloy have been a first successful attempt towards obtaining kinetic measurements at lower activation energies, and provide evidence of increasing curvature of the overall Q_a vs $\Delta G_{\text{tot}}^{\gamma\to\alpha'}$ relationship.

A curvature in the activation energy versus driving force function is in fact expected, since martensitic transformation is a barrierless heterogeneous reaction, controlled by interface mobility. Recently, experiments on certain nonferrous Cu–Al–Ni alloys [39] have also shown a nonlinear Q_a vs $\Delta G_{\text{tot}}^{\gamma\to\alpha'}$ functionality.

Table 3. Activation volume for martensitic transformation

Alloy	Activation volume
Fe–29.6%Ni [37]	~370 atoms
Fe–22.5%Ni–4%Mn [37]	~100 atoms
Fe–24%Ni–3%Mn [31]	~190 atoms
Fe–32%Ni–0.035%C (present investigation)	~60 atoms

5. CONCLUSIONS

1. It is shown that tensile hydrostatic stresses produced by the reflection of a shock wave at a free surface induce martensitic transformation in the Fe–32wt%Ni–0.035wt%C alloy above the ambient pressure M_s. Compressive stresses do not induce martensitic transformation.

2. Quantitative metallography results reveal that the fraction of martensite transformed increases with the decrease in temperature at a constant pulse duration; and with increase in pulse duration at a constant temperature. This time-dependence of martensitic transformation (which is considered to be athermal in the Fe–Ni–C alloys), proves the isothermal behavior of the transformation kinetics in the microsecond regime.

3. Lenticular martensite with a twinned mid-rib typical of bursting alloys is observed. The mean volume of a martensite plate is insensitive to temperature, pulse duration, stress, and the amount of martensite. This behavior is correlated with the autocatalytic spreading of clusters.

4. The activation energies for the transformation in the Fe–32wt%Ni–0.035wt%C alloy were calculated using a modified version of Pati and Cohen's equation incorporating variable saturation in the maximum fraction transformed. The values of the activation energies computed using this kinetic model range from 38,000 J/mol at -10°C to 25,000 J/mol at -60°C.

5. The activation energy exhibits a linear relationship with the total driving force (chemical driving force + mechanical work). The slope of the activation energy–total driving force plot gives the activation volume, which was found to be equal to approximately 60 atoms (0.7 nm^3). This value indicates that the rate controlling step for martensitic nucleation, in the Fe–32wt%Ni–0.035wt%C alloy, under the imposed conditions, is the mobility of the austenite–martensite interface.

6. The instrumented gas-gun experiments revealed an unexpectedly low wave velocity, indicative of lattice instability.

Acknowledgements—The authors wish to express their appreciation to Mr D. C. Erlich and P. S. DeCarli of SRI-International for conducting the gas-gun experiments. The assistance of Dr A. D. Romig Jr, Sandia National Laboratories, with the heat treatment and electron probe microanalysis of the alloy, and of Dr R. J. Salzbrenner, Sandia National Laboratories, for rolling the alloy is gratefully acknowledged. Dr G. B. Olson, Massachusetts Institute of Technology, discussed the results and contributed significantly to the analysis of the transformation kinetics. Professor J. C. Shyne, Stanford University, provided the Fe–32wt%Ni–0.035wt%C alloy. This research was supported by the National Science Foundation under Grant No. DMR 81-15127.

REFERENCES

1. V. Raghavan and A. R. Entwisle, Iron Steel Inst., Special Rep. No. 93, 30 (1965).
2. C. L. Magee, In *Phase Transformations*, Am. Soc. Metals, p. 115. Metals Park, Ohio (1970).
3. V. Raghavan and M. Cohen, *Metall. Trans.* **2**, 2409 (1971).
4. A. R. Entwisle, *Metall. Trans.* **2**, 2395 (1971).
5. G. V. Kurdjumov and O. P. Maksimova, *Dokl. Akad. nauk. U.S.S.R.* **61**, 83 (1948); **73**, 95 (1950).
6. S. C. Das Gupta and B. S. Lement, *Trans. Am. Inst. Min. Engrs* **191**, 727 (1951).
7. S. A. Kulin and G. R. Speich, *Trans. Am. Inst. Min. Engrs* **194**, 258 (1952).
8. E. S. Machlin and M. Cohen, *Trans. Am. Inst. Min. Engrs* **194**, 489 (1952).
9. R. E. Cech and J. H. Hollomon, *Trans. Am. Inst. Min. Engrs.* **197**, 685 (1953).
10. J. Philibert and C. Crussard, *J. Iron Steel Inst.* **180**, 39 (1955).
11. R. B. G. Yeo, *Trans. Am. Inst. Min. Engrs* **224**, 1222 (1962).
12. A. V. Anandaswaroop and V. Raghavan, *Sci. Met.* **3**, 221 (1969).
13. S. R. Pati and M. Cohen, *Acta metall.* **17**, 189 (1969).
14. E. Scheil, *Z. Anorg. allgem. Chem.* **207**, 21 (1932).
15. J. R. Patel and M. Cohen, *Acta metall.* **1**, 531 (1953).
16. M. A. Meyers and J. R. C. Guimarães, *Mater. Sci. Engng* **24**, 289 (1976).
17. E. O. Snell, J. C. Shyne and A. Goldberg, *Metallography* **10**, 299 (1977).
18. M. A. Meyers, *Metall. Trans.* **10**, 1723 (1979).
19. P. C. Maxwell, A. Goldberg and J. C. Shyne, *Metall. Trans.* **5**, 1305 (1974).
20. J. R. C. Guimaraes, Ph.D. thesis, Stanford Univ. Stanford, Calif. (1969).
21. N. N. Thadhani, Ph.D., dissertation, New Mexico Inst. Min Technol, Socorro, p. 70 (1984).
22. R. T. Dehoff and F. N. Rhines, *Quantitative Microscopy*, p. 52. McGraw-Hill, New York (1968).
23. R. L. Fullman, *Trans. Am. Inst. Min. Engrs* **197**, 447 (1953).
24. L. M. Barker, *SWAP-7, A Stress Wave Analyzing Program, Sandia* Nat. Lab. Albuquerque, SC-RR-67-143 (1967).
25. M. A. Meyers and C. T. Aimone, *Prog. Mater. Sci.* **28**, 1 (1983).
26. K. Tsuzaki and G. B. Olson, unpublished research.
27. N. N. Thadhani, M. A. Meyers and D. C. Erlich, *J. appl. Phys.* **58**, 2791 (1985).
28. I. Tamura, T. Maki and H. Hato, *Trans. J. Iron Steel Inst.* **10**, 165 (1970).
29. D. G. McMurtrie and C. L. Magee, *Metall. Trans.* **1**, 3185 (1970).
30. J. R. C. Guimarães and J. C. Gomes, *Metall. Trans.* **10**, 109 (1979).
31. S. R. Pati and M. Cohen, *Acta metall.* **19**, 1327 (1971).
32. G. B. Olson, M.I.T., Cambridge, Mass., private communications (1984).
33. L. Kaufman and M. Cohen, *Prog. Metal. Phys.* **7**, 165 (1958).
34. L. Kaufman and H. Nesor, *Z. Metall.* **64**, 249 (1973).
35. L. Kaufman, in *Metall. Chem. Symp. Proc.* (edited by O. Kubaschewski), p. 373. H.M.S.O., London (1972).
36. L. Kaufman and H. Nesor, *Calphad* **2**, 295 (1978).
37. M. Korenko, D.Sc. thesis, M.I.T., Cambridge, Mass (1973).
38. H. Knapp and U. Dehlinger, *Acta metall.* **4**, 289 (1956).
39. G. B. Olson and M. Cohen, in *Dislocations in Solids* (edited by F. R. N. Nabarro). To be published.
40. H. M. Ledbetter and R. P. Reed, *J. Phys. Chem.* Ref. Data **4**, 5351 (1973).
41. G. A. Alers, J. R. Neighbours and H. Sato, *J. Phys. Chem. Solids* **13**, 40 (1960).
42. A. Kanrav and U. S. Ghosh, *J. appl. Phys.* **52**, 5851 (1981).
43. H. M. Ledbetter, *J. appl. Phys.* **57**, 5069 (1985).
44. U. S. Ghosh and A. Kanrav, *J. appl. Phys.* **57**, 5071 (1985).

APPENDIX

SWAP-7 Computer code for obtaining stress profiles [24]

SWAP-7 (Stress Wave Analyzing Program) can be used to analyze problems involving shock waves in one-dimensional strain configuration in elastic–plastic solids. The method of characteristics used by SWAP-7 is applied to the numerical solution of hyperbolic systems of equations. In this method, the finite difference approximation is applied to the compatibility equations rather than to the original partial differential equations.

Shock wave problems in one-dimensional strain can be best visualized by making a plot of position vs time (distance–time plot) to describe the material history. A method of characteristics solution consists of determining the shock, free surfaces and interface paths on the distance–time plots, plus defining such quantities as stress, strain, pulse duration, and material velocity at all points.

To start the problem, the computer is given a set of initial conditions consisting of a mathematical description of all lines existing on the distance–time plane at some initial time, plus the equations of state of the materials involved.

In order to obtain the Hugoniot constants (bulk sound velocity C_0 and empirical parameter S which determines the linear relationship between the particle and shock velocities) in the equation of state, an instrumented gage experiment with the Fe–32wt%Ni–0.035wt%C alloy was performed. Two piezo-resistive manganin foil gages were sandwiched between three discs 2.5, 5.0, and 5.0 mm thick and 90 mm in diameter, which acted as the target (Fig. A1). A flyer plate of the same alloy (thickness of 2.5 mm and diameter of 56 mm) impacted the target assembly at a velocity of 72.8 m/s. The manganin gage read-out obtained for the Fe–Ni–C alloy, after converting voltage into stress, is shown in Fig. A2. A Lagrangian analysis of these gage read-outs was performed at SRI-International and the result is shown as a plot of particle velocity versus stress (Fig. A3). The lower particle velocities are attributed to the low bulk modulii observed in FeNi Invar type alloys [40]. Using the shock velocity analysis and with the velocities of impact for each event, the computer determines the interactions occurring upon impact, solves them, and modifies the picture on the distance–time plane to fit the new conditions. Information concerning each interaction is printed out leading to an output consisting of a chronological description of the

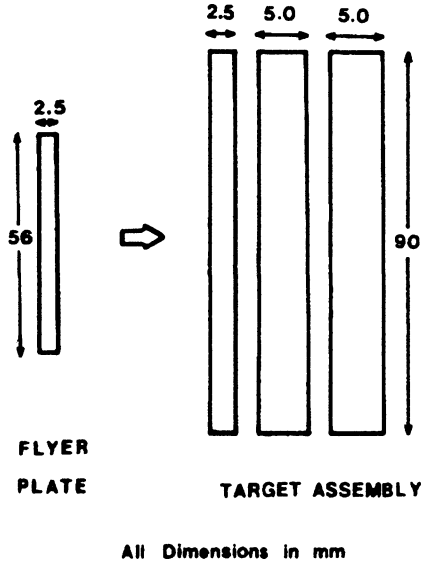

Fig. A1. Flyer plate and target assembly used for an instrumented gage experiment.

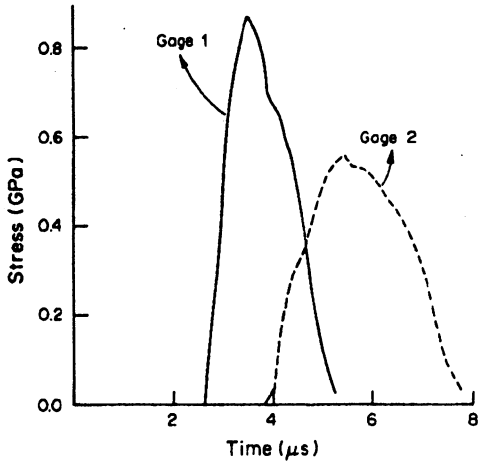

Fig. A2. Instrumented manganin gage read-out for Fe–32%Ni–0.035%C alloy after conversion of voltage into stress.

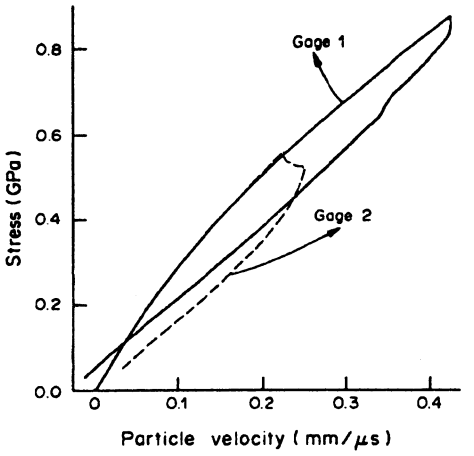

Fig. A3. Plot of stress vs particle velocity obtained by Lagrangian analysis.

events which occur in the problem. Representative distance–time plot (a) and stress–time plots (b, c, d) for the Fe–Ni alloy target impacted by a flyer of same material are illustrated in Fig. A4. The magnitudes and durations of tensile stress pulses can be obtained from these plots.

The bulk sound velocities obtained from the two gas-gun experiments are both consistently low; 2.6 mm/μs. By interpolating the bulk sound velocities of iron and nickel, one obtains a value of 3.9 mm/μs. The bulk sound velocity is dependent on Young's modulus and density. Changes in the elastic constants (C_{11}, C_{12}, C_{44}) that would result in the lowering of E could be responsible for the low bulk sound velocities. Nonlinear variation in the elastic constants with composition in Fe–Ni alloys is well known. Ledbetter and Reed [40] report Young's moduli (Fig. 5) for iron–nickel alloys. While Young's moduli for iron and nickel are equal to 210 and 220 GPa, respectively, an Fe–32 (wt%) Ni alloy has $E = 156$ GPa. These elastic instabilities have also been studied by Alers *et al.* [41] and Kanrav and Ghosh [42]. Recently, there has been some debate regarding this instability [43, 44]. This instability could be due to either magnetic/electronic structure changes, or the f.c.c.–b.c.c. transformation, or both. It is interesting that it reflects itself in a lower shock-wave velocity. Systematic experiments where wave profiles and velocities are determined could yield new information on martensitic nucleation; the shear instabilities observed could be due to the "softening".

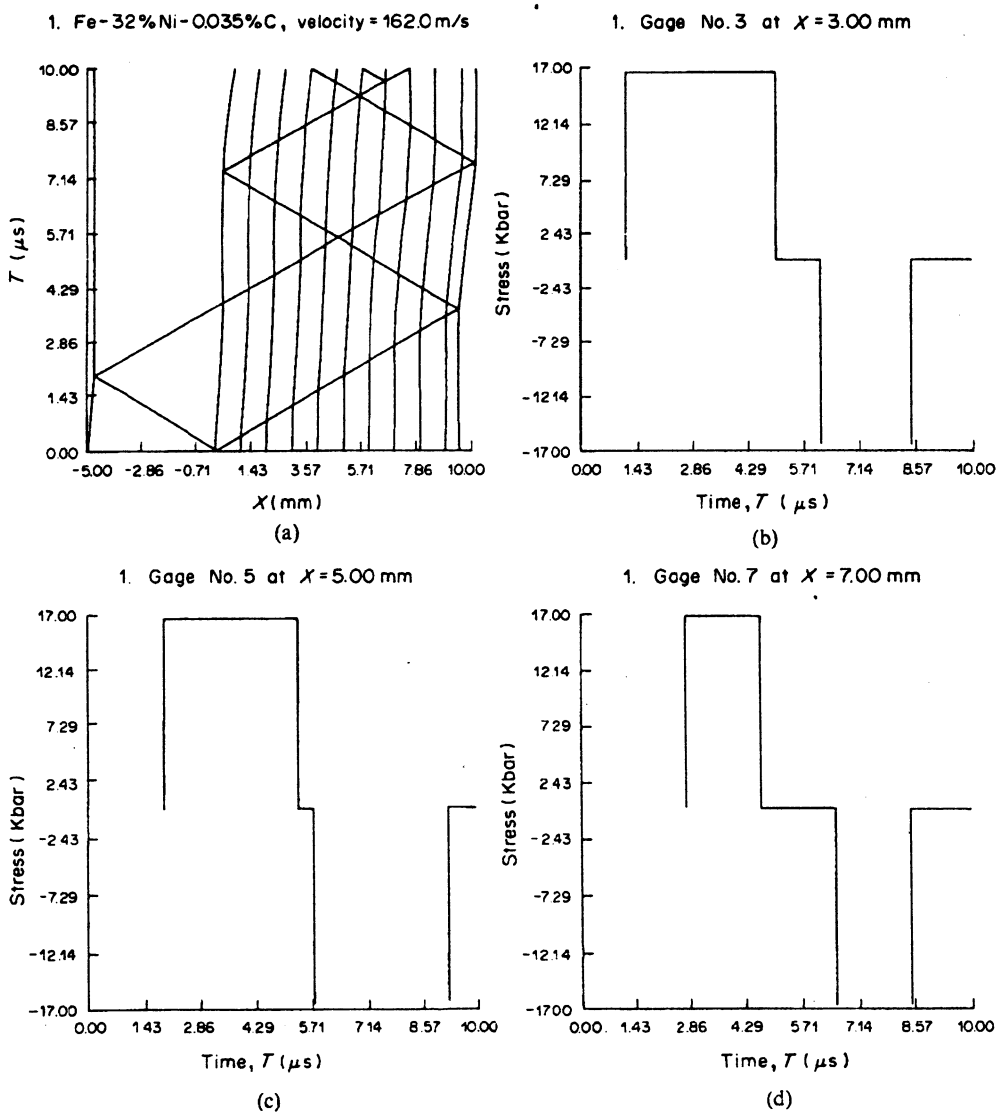

Fig. A4. (a) Distance–time plot of Fe-Ni-C alloy target impacted by flyer of same material. (b), (c), (d) stress profiles at 3.0, 5.0, and 7.0 mm away from impact surface.